Chasing the Cut: A Measurement Approach for Machine Tool Condition Monitoring

Łukasz Huchel, Thomas C. Krause, Tomasz Ługowski, Steven B. Leeb, *Fellow, IEEE*, and Jan Helsen

***Abstract*— Often, the condition of a machine tool is detected indirectly in the reduced quality of manufactured parts upon visual inspection. Reliable and efficient machine tool condition monitoring is indispensable for manufacturing. Furthermore, issues affecting machine tools are closely related to pathologies associated with many other industrial electromechanical systems. An instrumentation and measurement solution for tool condition monitoring is presented in this article. A signal processing algorithm and instrumentation hardware are proposed to avoid intrusive sensor installations or modifications of the machine under test. The cyclostationary properties of machine vibration signals drive fault-detection approaches in the proposed sensing hardware and signal processing chain. A sample of end mills from an industrial facility is used to validate the tool condition monitoring system.**

***Index Terms*— Cyclostationarity, diagnostics, integrated electronic piezoelectric (IEPE), Internet of things (IoT), spectral coherence, tool condition monitoring (TCM), WiFi.**

I. Cutting to the Chase

MACHINED material is the backbone of humankind's most impressive and useful innovations. Manufactured goods ranging from keys to ships are still primarily assembled with parts created by removing raw material with cutting tools. For example, end mills remove material radially and axially. They are used in face milling, peripheral milling, and slot milling. Cutting tool condition directly affects finish quality and safety, e.g., the likelihood of tool breakage or kickback [1]. Currently, human operators rely on heuristic techniques, visual inspection of the tools, bits, or machined parts, and experience, to decide when tools have reached the end of their life-cycle. Computer-based tool condition monitoring (TCM) systems provide the opportunity for more accurate condition diagnosis. These systems are increasingly important as machining processes transition to fully autonomous operation. Tool condition monitoring enables the Industry 4.0 revolution and the potential application of the Internet of things (IoT) devices in many manufacturing operations. This article introduces a robust condition metric based on spectral coherence in easily acquired vibration signals. Results are demonstrated using end mills from real manufacturing operations, but the approach presented in this article applies more generally to any cutting machine tool and other industrial electromechanical systems with the periodic operation, including lathes, compressors, a variety of pumps, and other machines.

Monitoring systems that permit accurate fault detection and diagnostics (FDD) with easy installation remote from the direct machining area would enhance safety, reliability, and flexibility in gathering actionable process information. References [2]–[5] analyze the examination of acoustic and vibration signatures for tool condition monitoring (TCM). These methods are useful for TCM, but they employ invasive measurement setups that are not always practical. For example, the setup presented in [2] requires an acoustic emission sensor to be mounted very close to the workpiece. In [6], three accelerometers are mounted directly on the vice that clamps the workpiece, a serious limitation in industrial environments that expect flood cooling, quick workpiece changes, and highly automated procedures. Force and tool position measurements have been utilized in [1] and [7] for the diagnosis of tool wear. Lins *et al*. [8] use image analysis for drilling machine TCM. All of these methods may be stymied by the use of coolant or a requirement for distanced sensor installation from the cutting area.

Generally, approaches for cutting tool diagnostics fall into one of two categories. The first approach uses analytical signal processing algorithms to obtain condition metrics. The second approach identifies tool diagnostics as a classification problem and uses machine learning tools. Both time and frequency domain signal processing have been used for TCM [5], [9], [10]. Frequency domain signal processing is attractive because of the rich harmonic content and associated modulation components of measured signals in many machining operations. Many spectral or related decompositions have been applied, including various Fourier methods and also wavelet analysis [5], [11]. Short time or windowed decompositions like the short-time Fourier transform and the wavelet transform provide time localization [11], potentially valuable for analyzing nonstationary signals such as cutting scenarios with small work pieces or intermittent cutting. Cepstrum analysis presents great potential for the separation of system response and excitation [12], [13]. The properties of

Manuscript received November 15, 2020; accepted December 10, 2020. Date of publication December 29, 2020; date of current version February 2, 2021. This work was supported in part by the Office of Naval Research Structural Acoustics Program and in part by the Fulbright Foundation. The Associate Editor coordinating the review process was Dr. Datong Liu. *(Corresponding author: Łukasz Huchel.)*

Łukasz Huchel, Thomas C. Krause, and Steven B. Leeb are with the Department of Electrical Engineering and Computer Science, Massachusetts Institute of Technology, Cambridge, MA 02139 USA (e-mail: lhuchel@mit.edu; tkrause@mit.edu; sbleeb@mit.edu).

Tomasz Ługowski resides in Bielsko-Biała, Poland (e-mail: lugowski@autograf.pl).

Jan Helsen is with the Vrije Universiteit Brussel/OWI-lab, 1050 Brussel, Belgium (e-mail: jan.helsen@vub.be).

Digital Object Identifier 10.1109/TIM.2020.3047939

the complex logarithm make cepstrum-based TCM approaches less sensitive to sensor placement but more susceptible to noise [14]. The spectral correlation (SC) function can be used to explore the cyclostationary features of signals associated with milling [6]. Periodic excitation at the cutting frequency, amplitude modulation due to tool symmetry, and other phenomena related to material removal create multiple cyclostationary signals [15]. In [16], the authors apply cyclostationary analysis to monitor chatter in high speed milling. Calleecharan [17] investigates the effect of force modulation of the boring bar in a lathe. The performance of cyclostationary analysis is compared with conventional spectral analysis. Application of SC for TCM is described in [6]. SC provides powerful opportunities for finding faults in periodic operations, e.g., the rotation of a mill cutter. However, these methods are usually applied to synchronously sampled data in order to align spectral frequency "bins" with the periodicity, e.g., rotation of the cutting tool. A quadrature encoder is attached, for example, to the machine spindle to synchronize sampling, a costly and invasive installation technique.

The classification approach to condition monitoring has grown in popularity with the increased interest in machine learning methods. Growth in computational power, data storage, and interest for machine learning methods have contributed to this rise in popularity. For example, in [18], continuous wavelet transform scalograms of vibration signals from rotating machinery are fed to a convolutional neural network (CNN) to produce good fault signatures and diagnostic indicators. In [19], a CNN and images of machining tools are used to diagnose tool wear. CNNs have been used to predict important parameters such as the remaining useful life of a mechanical tool [20]. These techniques require subject experts to train models and tune parameters. These methods produce heavy computation burdens in training and operation. It is always difficult or impossible to guarantee the response to situations that were not considered or "covered" by the training data.

This article proposes an instrumentation and measurement solution to condition monitoring for periodic operations like milling. The custom embedded hardware interfaces with common industrial accelerometers. The signal processing approach employs cyclostationary analysis tools to reveal hidden features of the vibration signature. Cyclostationary analysis is one of the analytical TCM methods that has presented high potential and gained acceptance [6], [16]. Despite the great characteristics of analytical methods, they are under explored. A recent survey of milling TCM approaches [10] showed a disproportional interest in classification methods. As a result, cyclostationary-based TCM lacks a normalized figure of merit and statistical verification. To address these shortcomings, a new normalized indicator is considered. The proposed tool condition indicator is demonstrated on a sample of end mills from an industrial facility. The impact of end mill mounting conditions and cutting parameters are also investigated. A discussion of this new figure of merit and its variation over multiple tests summarizes this work.

II. Chasing the Cut

Mechanical processes such as milling operations generate acoustic, vibration, and visual signals, all potentially useful for diagnostic indicators. Vibration sensing is a useful choice because of the availability of high bandwidth and high-quality sensors. They provide signals that are directly useful for fault and wear detection. Vibration signals do not demand the computational burden of image analysis or suffer from acoustic miscues. In this work, vibration signals drive the signal processing algorithm. However, other sensed signals, for example, acoustic signals, could serve as inputs to the methods developed here.

A. Cyclostationary Analysis

Most mechanical systems generate periodic vibration signatures [21]. The vibration content can be divided into a so-called "predictable part," caused by fundamental actions such as shaft rotation and gear meshing, and also a "random part," i.e., content hard to describe analytically with a deterministic model [15]. Oftentimes, the predictable part of the signal imposes various forms of modulation on the random part. An example is shown in [22], where modulation is caused by the pumping frequency of a positive displacement pump. The nonstationary stochastic nature of the signal arises from the interaction between the predictable and random parts [15], [23]. Powerful signal processing tools exist to deal with a class of nonstationary stochastic signals called cyclostationary signals. Cyclostationary signals have periodically time-varying statistical properties.

In machining applications, periodic modulation in the vibration signal arises as a cutting tool that removes material. The vibration produced by an end mill cutting operation, for example, is periodic due to the rotating spindle. For a given number of flutes, a cutting edge engages the material multiple times per spindle rotation. The resultant vibration in the machine presents both a predictable and random part. Cyclostationary analysis is a valuable signal processing tool for relating the periodicities to the cutting physics.

The theory of cyclostationary random processes can be understood from at least two perspectives, either using time averages and statistical spectral analysis or ensemble averages, i.e., a probabilistic approach [24]. In this article, the time-average-based approach is used. The time-variant mean $\hat{M}_x(t)$ of a signal and the time-variant autocorrelation function $\hat{R}_x(t, \tau)$ are defined as

$$\hat{M}_x(t) = \lim_{N\to+\infty} \frac{1}{2N+1} \sum_{i=-N}^{N} x(t + i \cdot T_0) \tag{1}$$

$$\hat{R}_x(t, \tau) = \lim_{N\to+\infty} \frac{1}{2N+1} \times \sum_{i=-N}^{N} x\left(t + \frac{|\tau|}{2} + i \cdot T_0\right) \cdot x\left(t - \frac{|\tau|}{2} + i \cdot T_0\right) \tag{2}$$

where T_0 is the fundamental period and τ is a lag parameter. Computing the time-variant mean is commonly referred to

as synchronous averaging, also known as superposed epoch analysis [25]. Signals exhibiting a periodic time-variant mean, $\hat{M}_x(t) = \hat{M}_x(t+T_0)$, are called first-order cyclostationary [15]. Signals with a periodic time-variant autocorrelation function are called second-order cyclostationary [15]. Fourier series analysis can characterize the periodicity of the time-variant autocorrelation function. The Fourier series synthesis equation can be written as

$$\hat{R}_x(t,\tau) = \sum_{m=-\infty}^{+\infty} \hat{R}_x^{\frac{m}{T_0}}(\tau) e^{j2\pi m/T_0 t} \tag{3}$$

where $\hat{R}_x^{(m/T_0)}(\tau)$ is the mth Fourier coefficient, also known as the limit cyclic autocorrelation function. Equations (2) and (3) conclude that $\hat{R}_x^{(m/T_0)}(\tau)$ describes the periodic components of the lag-product time-series $x(t+(|\tau|/2)) \cdot x(t-(|\tau|/2))$. The Fourier series analysis formula is applied to $x(t+(|\tau|/2)) \cdot x(t-(|\tau|/2))$ to define as

$$\hat{R}_x^{\frac{m}{T_0}}(\tau) = \lim_{T\to+\infty} \frac{1}{T} \int_{\frac{-T}{2}}^{\frac{T}{2}} x\left(t+\frac{|\tau|}{2}\right) \cdot x\left(t-\frac{|\tau|}{2}\right) e^{-j2\pi m/T_0 t} dt. \tag{4}$$

The periodogram–correlogram relation is applied to the limit cyclic autocorrelation function, and substituting $\alpha = (m/T_0)$, the limit cyclic spectrum is obtained as

$$\hat{S}_x^{\alpha}(f) = \mathcal{F}\left(\hat{R}_x^{\alpha}(\tau)\right). \tag{5}$$

Equation (5) is represented as a bifrequency map, where the first axis is the cyclic frequency α and the second axis is the center frequency f [26]. The cyclic frequency α reveals modulation in the signal of interest, an extremely valuable feature in mechanical system diagnostics. However, in such applications, an alternative interpretation of the limit cyclic spectrum is used. The SC function is defined using the following signal definitions: $v(t) = x(t)e^{j\pi\alpha t}$, $u(t) = x(t)e^{-j\pi\alpha t}$ and statistical spectral analysis [25], [27]:

$$\hat{S}_x^{\alpha}(f) = \lim_{T\to+\infty} \lim_{\Delta t\to+\infty} \frac{1}{\Delta t}\frac{1}{T} \times \int_{-\Delta t/2}^{\Delta t/2} X\left(u, f+\frac{\alpha}{2}\right)_T \cdot X^*\left(u, f-\frac{\alpha}{2}\right)_T du \tag{6}$$

where $X(t,f)_T$ is a time-variant finite-length Fourier transform of $x(t)$ [27]. Equation (6) provides temporal correlation values for frequency components shifted by α. For example, the SC function presents high values due to sidebands from modulation with frequency α.

The SC function exposes potential modulation and hidden periodicities in random signals. It also has the benefit of noise immunity. For a stationary noise signal, the time-variant autocorrelation function $\hat{R}_x(t,\tau)$ has no t dependence, $\hat{R}_x(t,\tau) =$ const $\forall t$. Consequently, values of $\hat{R}_x^{\alpha}(\tau)$, the Fourier series coefficients of $\hat{R}_x(t,\tau)$, are zero for all frequencies other than dc, i.e., $\alpha \neq 0$. In other words, contributions to the SC function due to stationary noise are limited only to the line $\alpha = 0$. Based on this observation and (5), SC presents high immunity to stationary noise [23]. In conventional spectral analysis ($\alpha = 0$), additive stationary noise can mask the potential signal of interest.

B. Spectral Coherence

Different types of mechanical systems generate vibration signals at very different energy levels, but often the signals contain similar modulation features. It is of great interest to develop a condition indicator that is agnostic to energy scaling effects. A normalized indicator avoids false triggering due to varying energy levels, e.g., due to different loading conditions or system size. To address this, the spectral coherence coefficient $\gamma_x^{\alpha}(f)$ is applied as

$$\gamma_x^{\alpha}(f) = \frac{\hat{S}_x^{\alpha}(f)}{\sqrt{\hat{S}_x^0\left(f-\frac{\alpha}{2}\right)\hat{S}_x^0\left(f+\frac{\alpha}{2}\right)}}. \tag{7}$$

In general, $\gamma_x^{\alpha}(f)$ is a complex quantity with magnitude $|\gamma_x^{\alpha}(f)| \leq 1$. The coefficient provides a measure of cyclostationarity and is agnostic to scaling effects. For example, two time-varying processes with different energy levels can be reliably compared. In [22], authors introduce a spectral coherence-based indicator for diagnostics. The mean envelope spectrum (MES) $S_x^{\langle f\rangle}(\alpha)$ is defined as follows:

$$S_x^{\langle f\rangle}(\alpha) = \frac{1}{|F|}\int_F |\gamma_x^{\alpha}(f)| df \tag{8}$$

where $|F|$ is the range of integration over center frequencies. The MES is a vector quantity and serves as the input to a new figure of merit described in Section VI.

III. Diagnostic Hardware

The noise-rejecting properties of the SC ease the burden of sensor placement. For example, for a mill cutter, as flutes become damaged, a periodic component is introduced or enhanced in the vibration signature of the machine. Examination of the SC and the associated MES indicator relieves the burden of attempting to make physically close, synchronized measurements directly on the cutting process. We have developed custom instrumentation to exploit these benefits. The wireless data-acquisition device is compatible with integrated electronic piezoelectric (IEPE)-based accelerometers, state-of-the-art high bandwidth current-loop piezoelectric vibration sensors. Remote processing power and nonvolatile memory enable selective measurement and storage of raw vibration time-series data.

The custom instrumentation offers benefits in data acquisition, detection, and nonintrusive sensing. There are four simultaneously sampled differential channels that can serve IEPE accelerometers, the *de facto* industry standard for high fidelity vibration measurement. A $\Delta\Sigma$ ADC supports sampling rates up to 128 kHz and a programmable resolution of 16 or 24 bits. The wireless connection is used for data transfer and is compatible with IEEE 802.11. The device can operate as either an access point (AP) or a WiFi station (STA). A wired serial connection is also provided for basic device configuration and diagnostics. Nonvolatile memory and a real-time clock enable a lightweight data management system. Files are stored using the standard FAT file system to comply with most modern operating systems. The device operates as a server, clients can check files in the remote memory, download files, delete files, and ask for new data to be acquired.

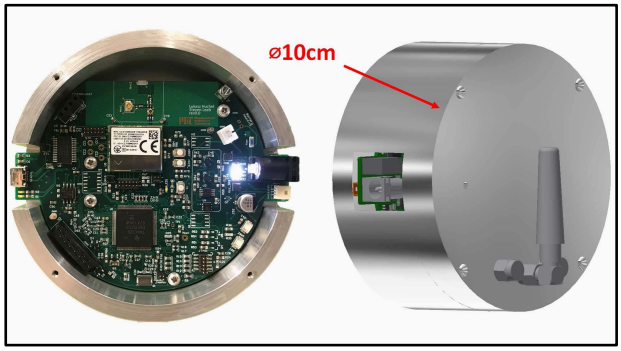

Fig. 1. View of proposed embedded system.

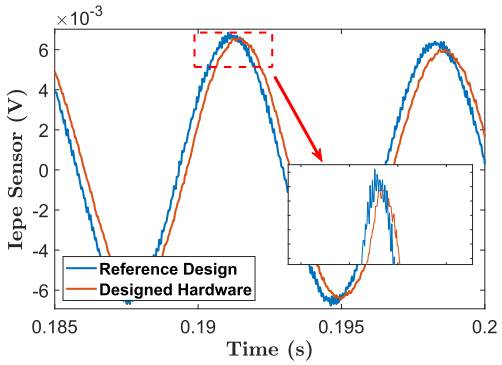

Fig. 2. Sample vibration signal.

Sensitive instrumentation and small device footprint permit flexible mounting conditions and the detection of subtle, early diagnostics in machine tools and similar mission critical machinery. Fig. 1 presents a view of the proposed industrial monitor, the small size is evident. A temporary, nonintrusive mounting scenario is shown by the experimental setup in Fig. 2. Magnets embedded in the case hold the device to ferromagnetic materials, e.g., the body of a milling machine. The data acquisition device can be powered from a conventional 5-W wall adapter or 3.7-V battery for temporary deployment. The compact custom instrumentation supports a nonintrusive measurement approach that preserves environmental barriers and safety.

As an example of the benefits offered by the custom instrumentation, a comparison with an IEPE acquisition platform built according to the guidelines in [28] is shown in Figs. 2 and 3. IEPE devices are excited by a dc current source. Comparisons presented in Figs. 2 and 3 reveal that the current source implementation of the reference design introduces significant high frequency noise into the measurements. The noise contribution is large enough to have a visible effect on the vibration and acoustic signals even in the time domain representation.

The results shown in Figs. 2 and 3 present the vibration and acoustic signals emitted by a speaker excited at a pure tone, respectively. The noisy measurements from the reference hardware are shown in blue and measurements from the custom instrumentation are shown in red. Both measurements were performed with the same sampling frequency and bit

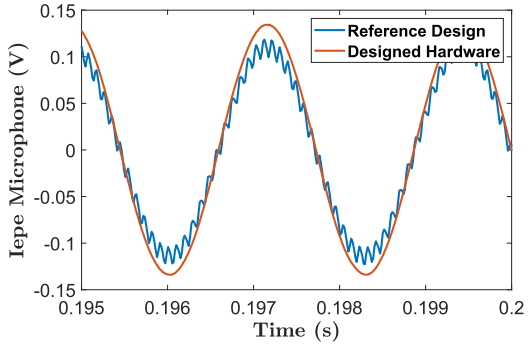

Fig. 3. Sample acoustic signal.

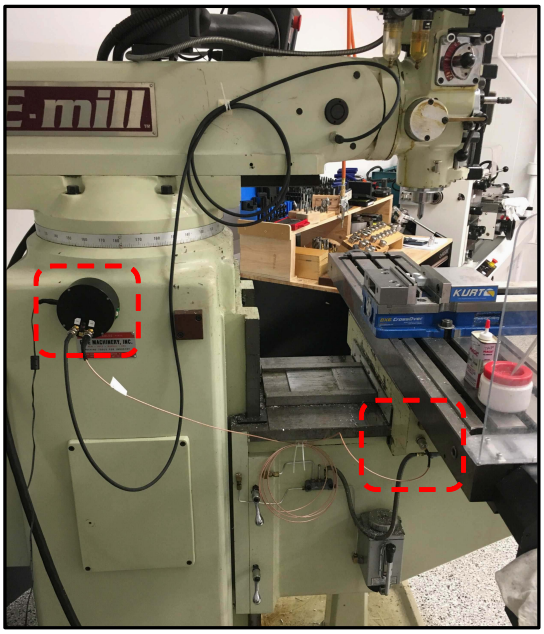

Fig. 4. View of experimental setup.

resolution. The improvements enable full utilization of the high sampling rate and resolution of the device for TCM.

IV. Experimental Setup

A vertical Bridgeport-style milling machine was used as a testbed. CNC capability was necessary to achieve desired and repeatable cutting parameters. Three different types of cutting tools were used in the experiment: 4-flute 6-mm, 8-mm, and 0.25-in carbide end mills. The acquisition device and sensor mounting points are marked in Fig. 4. The sensor is mounted on the bottom of the table. This sensor position is fixed for all of the experiments presented here. Note that this or a similar sensor location, isolated from the cutting action, is very practical for production environments. Experimental results confirm that the remote sensor location can provide data to successfully diagnose bit condition. Experimental setup details are provided in Table I. Peripheral cuts with a varying axial depth of cut (ADOC), radial depth of cut (RDOC), and feed rate were considered. Two different tool mounting conditions were tested: R8 collets and ER16 collets.

TABLE I
SETUP DETAILS

Parameter	Value
Mill	ACER EVS-3VKH
Accelerometer	Wilcoxson 728T
Stock material	Aluminium
Stock grade	6061
6 mm end mill	WNT 54005060
8 mm end mill	WNT 54006080

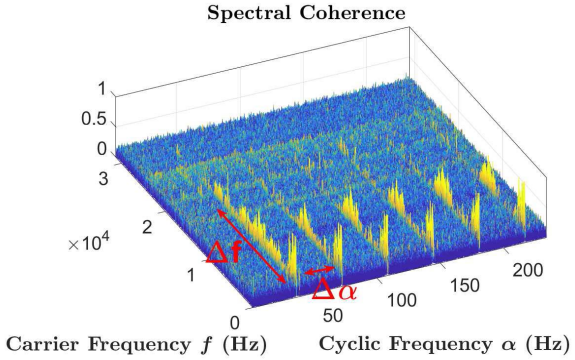

Fig. 5. Spectral coherence map for sample vibration data.

V. ARTIFICIAL BIT DEGRADATION

To provide an illustrative application, as a demonstration, the MES was developed for vibration signatures of 0.25-in end mills in a peripheral cut scenario. A spectral coherence map for a 0.25-in end mill is presented in Fig. 5. The ordinate corresponds to carrier frequency f, while the abscissa corresponds to cyclic frequency α. In this experiment, the spindle speed was set to 2150 rpm. It can be seen that spectral coherence is a discrete function of frequency α, and a continuous function of frequency f. The continuity of the spectral coherence in f reveals the presence of random content in a wide frequency range [15]. Cyclic components are present at multiples of the spindle frequency, with spacing $\Delta\alpha = (2150/60) \approx 36$ Hz. Evaluation of the MES involves the integration of spectral coherence along frequency f, (8), the direction of integration is marked in Fig. 5 with Δf. The integration will convert the 2-D spectral coherence map into the 1-D quantity of MES. However, as observed in Fig. 5, only a discrete set of frequencies α are meaningful, i.e., there are countable components due to cyclic operation. The MES will be represented with a bar plot.

To provide more intuition for the MES, a numerical experiment is conducted and compared with laboratory results. Four cases are considered: a new end mill and three degraded end mills. The degraded end mills are characterized as follows: one flute removed, two adjacent flutes removed, and two opposite flutes removed. Fig. 6 presents an axial view of the end mills. The red outlines highlight the artificial degradation imposed on the tools. The simulated vibration signal for each scenario is presented in Fig. 7. The red envelope represents the amplitude modulation signal applied to the random carrier. The symmetry of the modulation signal in each case corresponds to the

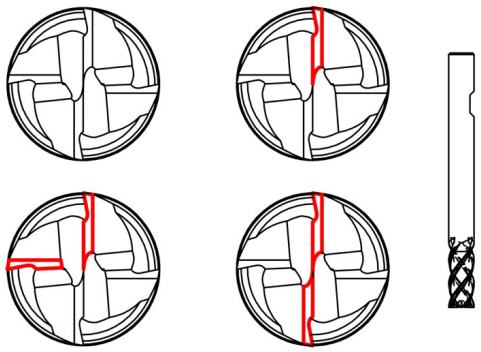

Fig. 6. Artificial end mill degradation.

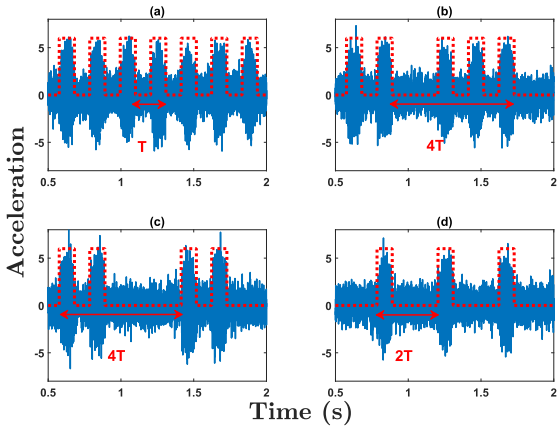

Fig. 7. Simulated signal for the artificial degradation experiment: (a) new tool, (b) one flute removed, (c) two adjacent flutes removed, and (d) two opposite flutes removed.

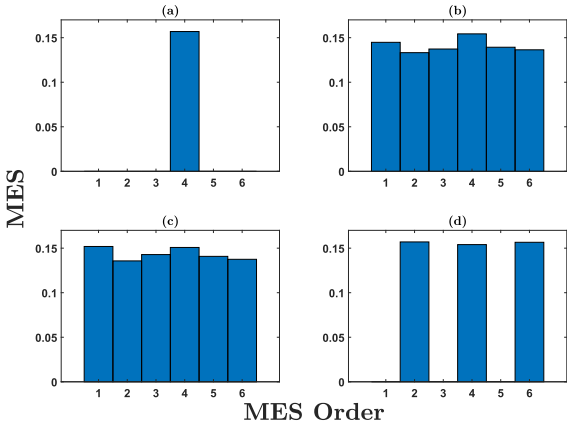

Fig. 8. MES for simulated data: (a) new tool, (b) one flute removed, (c) two adjacent flutes removed, and (d) two opposite flutes removed.

engagement of the end mill cutting surface. The scaling of the signal is not important, the temporal features are of interest. The time period T corresponds to the modulation period of the healthy four flute tool. Other modulation periods are expressed in terms of T. The MES for each simulated case is presented in Fig. 8. The horizontal axis is modified from *Hz* to *orders*. The first order corresponds to an event that occurs once per spindle revolution, which rotates at a frequency of 36 Hz.

Orders correspond to cyclic frequencies, i.e., frequencies of modulation. Therefore, an inherently related and easily observable quantity, the period of modulation, is analyzed.

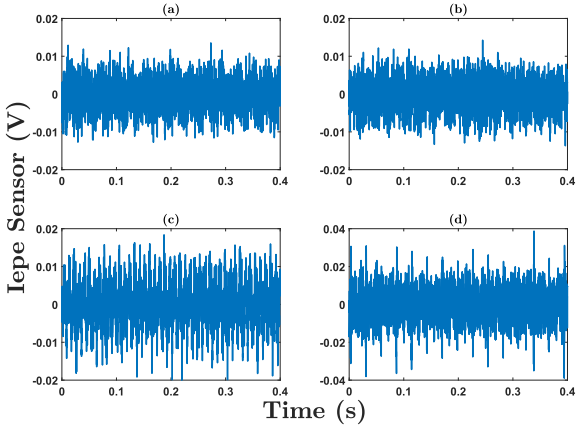

Fig. 9. Vibration signal for artificial degradation experiment: (a) new tool, (b) one flute removed, (c) two adjacent flutes removed, and (d) two opposite flutes removed.

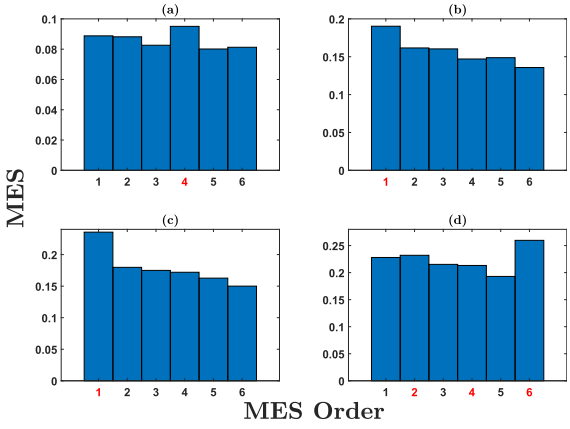

Fig. 10. MES for artificial degradation experiment: (a) new tool, (b) one flute removed, (c) two adjacent flutes removed, and (d) two opposite flutes removed.

The fundamental period varies between cases (a)–(d) and has a distinct impact on the MES bar plots. For a healthy tool, the modulation period occurs four times per spindle rotation. Thus, the fundamental MES component in Fig. 8(a) appears in the fourth order. However, for one flute removed and two adjacent flutes removed, the modulation period occurs once per spindle rotation. In those cases, the fundamental MES components in Fig. 8(b) and (c) appear in the first order. For the tool with opposite flutes removed, Fig. 8(d), the modulation period occurs twice per spindle rotation. The nonsinusoidal nature of modulation contributes to higher order MES components at integer multiples of the fundamental MES order. The above discussion provides necessary insight for further analysis of laboratory results.

Laboratory measurements were conducted on one new and three artificiality degraded end mills. For each case of "damage," the end mill flutes were hand ground on a bench grinder. Measured vibration signals for each of the cases (a)–(d) are presented in Fig. 9. Time domain interpretation of the signal content is difficult, i.e., the damage signatures in the measured signals are subtle and difficult to detect visually. In cases (c) and (d), some periodicity is visible as bursts in the vibration signal; however, any general modulation trend is hidden.

The MES presents exceptional and intuitive insight. The MES plots for each case are given in Fig. 10. It can be seen in Fig. 10(a) that for the new tool, the fourth order is dominant. However, contrary to the simulated case, the first order and its integer multiples are present. The lower orders appear due to imperfections in the original tool and the imposed degradation. The first order is dominant for cases (b) and (c), one flute ground and two adjacent flutes ground, respectively. This matches the observation from the simulation. Even orders are dominant for case (d), two opposite flutes ground. However, there is a distinct dominance of sixth order when compared to the simulation data. The exact replication of relative magnitudes between the simulation and the experiment is not expected. However, the trend of the MES indicator reveals the changes in degradation.

To further emphasize the benefits of the MES as a tool diagnostic indicator and justify the signal processing approach,

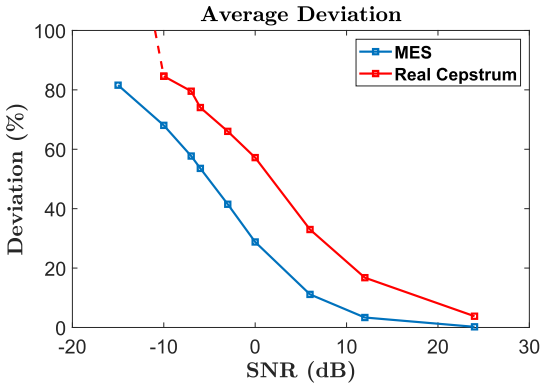

Fig. 11. Comparison of the average deviation for real cepstrum and MES.

a comparison with cepstrum is developed. The cepstral analysis is a valuable tool in the diagnostic of mechanical systems and speech processing [5], [13], [14]. For a given signal, the MES values of the first six orders contain important information. Similarly, for the cepstrum of a signal, the six lowest dominant frequency components are informative [13]. The average deviation of the first six MES values and six lowest dominant frequency components of the same vibration data of a milling process corrupted with noise is considered. White Gaussian noise with variance designed according to (9) is used in the analysis. By inspection of (9) the deviation from the case with no added noise is expected to approach zero with increasing SNR, e.g., a case with infinite SNR becomes the reference case. The results of the comparison are shown in Fig. 11. Each point in Fig. 11 corresponds to the average deviation of MES and cepstrum quantities

$$\sigma^2 = \frac{P_{\text{sig}}}{10^{\frac{\text{SNR}}{10}}} \tag{9}$$

where σ^2 is the noise variance, P_{sig} is the average power of the reference vibration data. The average deviation of MES is uniformly better across the SNR range. For SNR values below -10 dB, the deviation for cepstrum becomes excessively big, in fact, the frequency components cannot be distinguished from the noise floor. In this scenario, the MES continues to provide correct dominant components.

Simulation and experiments with intentionally damaged end mills, with flute surfaces marred to present a known

Fig. 12. Good and bad 8-mm carbide end mills.

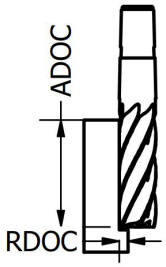

Fig. 13. Illustration of ADOC and RDOC.

pattern, demonstrate the utility of the MES for finding diagnostic indications in cyclic and carrier frequencies. Section VI extends this demonstration to end mills damaged by wear in a normal industrial environment. High noise immunity justifies the choice of MES as the diagnostic metric.

VI. Industrial Samples

The TCM system was tested with industrial end mill samples. Tools used in the experiment were retired from a CNC-based production line due to poor finish. A side by side comparison of new and worn samples is shown in Fig. 12. The distributed nature of the degradation is evident. Realistic wear is a complicated combination of multiple defects, including the simple cases from Section V. A useful condition indicator has to perform well in the complex realistic scenario. The vibration signatures of cuts with new and worn, 6- and 8-mm diameter industrial end mills were analyzed.

In milling applications feed rates and cut parameters are set to achieve optimal chip load, which is recommended by tool manufacturers. There are two common milling strategies that aim to achieve optimal chip load, traditional milling, and high efficiency milling (HEM). Traditional milling uses low ADOC, high RDOC, and slower feed rates. Contrary to that, HEM uses low RDOC, high ADOC, and higher feed rates [29]. The definitions of RDOC and ADOC are presented in Fig. 13 in a peripheral cut setup.

For each end mill, four peripheral cuts were analyzed. The cut parameters are listed in Table II. RDOC is expressed in terms of the percentage of the tool diameter. ADOC is expressed in terms of the percentage of tool cutting depth,

TABLE II
Optimal Cutting Parameters

Cut Number	Parameter		
	RDOC (% ⌀)	ADOC (% 2⌀)	Feed Rate (IPM)
Cut 1	40	50	15
Cut 2	5	50	30
Cut 3	10	100	30
Cut 4	5	100	45

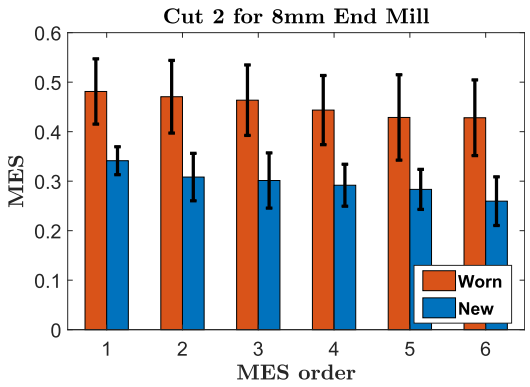

Fig. 14. Cut 2 comparison for 8-mm end mills.

which is typically twice the diameter. Feed rate is expressed in inches per minute. For example, Cut 1 with a 6-mm end mill results in the following values: 2.4-mm RDOC and 6-mm ADOC.

The parameters were chosen to achieve almost optimal chip load for both 6- and 8-mm diameter end mills. The parameters of Cut 1 are representative of a traditional milling strategy. The parameters of Cut 4 are representative of a HEM strategy. The parameters of Cut 2 and Cut 3 are not prime candidates of either strategy, but all configurations maintain almost optimal chip load.

The MES bar plot for Cut 2 with an 8-mm tool is presented in Fig. 14. The height of the bars represents the average value of MES for each order. The error bars represent two standard deviations. The sample mean and sample variance were evaluated with a sample of four independent cuts for each tool. With the assumption of Gaussian distribution and treating sample mean and sample variance as distribution parameters, 95.4% of possible MES values are located within the error bars in Fig. 14. Even without this assumption, a valid bound is provided using Chebyshev's inequality (10). This inequality can be applied to any distribution with defined mean and variance

$$\Pr(|X-\mu| \geq 2\sigma) \leq \frac{1}{4}. \tag{10}$$

Using (10), and treating sample mean and sample variance as distribution parameters, 75% of possible MES values are located within the error bars in Fig. 14.

The MES provides a valuable condition indicator, however, a scalar indicator is of bigger interest. A normalized figure of merit was missing in previous cyclostationary-based TCM literature. Simple threshold criteria can be applied to

TABLE III
MES TABLE FOR 6-mm TOOL

Cut Number	Worn		New		Ratio
	MESbI	σ	MESbI	σ	
Cut 1	2.76	0.15	1.76	0.08	1.57
Cut 2	3.12	0.12	2.05	0.18	1.53
Cut 3	2.84	0.05	1.96	0.06	1.45
Cut 4	3.21	0.06	2.08	0.08	1.55

TABLE IV
MES TABLE FOR 8-mm TOOL

Cut Number	Worn		New		Ratio
	MESbI	σ	MESbI	σ	
Cut 1	2.34	0.02	1.23	0.03	1.90
Cut 2	2.71	0.09	1.79	0.05	1.52
Cut 3	2.88	0.06	1.71	0.11	1.69
Cut 4	2.80	0.05	1.93	0.08	1.44

a single numeric value. We define a MES-based indicator (MESbI) as follows:

$$\text{MESbI} = \sum_{i=1}^{N} S_x^{(f)}(i\,\Delta\alpha) \tag{11}$$

where N is the total number of cyclic frequencies to be examined, $\Delta\alpha$ is the frequency spacing in the cyclic domain. For an idea of the relative MESbI variation between tests, the standard deviation of the MESbI is defined. Treating the MES values of each order as independent random variables, the standard deviation of the MESbI is defined in the following equation:

$$\sigma_{\text{MESbI}} = \sqrt{\sum_{i=1}^{N} \sigma^2(i\,\Delta\alpha)}. \tag{12}$$

Of course, independence in this scenario cannot be guaranteed and is not necessarily expected. In general, a joint probability distribution is necessary for variance analysis. Additionally, without pair-wise independence a covariance matrix is necessary to characterize the problem. The definition in (12) does not survive rigorous mathematical scrutiny, however, it still provides a useful indication of variability. Such information provides the potential user more insight. According to Fig. 14, very good separation of both cases can be achieved.

Tables III and IV provide MESbI, σ_{MESbI}, and ratios of indicators for new and worn cases. There is a significant increase in the MESbI value for degraded end mills. A 90% increase in the MESbI value is seen for Cut 1 of the 8-mm end mills. For 6- and 8-mm end mills, there is at least a 40% increase in the MESbI value from new to worn end mills.

The indicator proposed in this section is capable of diagnosing degraded end mills. In Section V, the MES was used for analysis of end mills with discrete and exaggerated damage.

TABLE V
MES TABLE FOR ER16 COLLET AND 8-mm TOOL

Cut Number	Worn		New		Ratio
	MESbI	σ	MESbI	σ	
Cut 1	2.03	0.04	1.20	0.04	1.69
Cut 2	2.87	0.06	2.07	0.03	1.39

A single numeric MES indicator facilitates simpler analysis. The MESbI proved to be a good indicator for industrially-worn end mills with a complex combination of defects. The repetitiveness of separation between cases was validated with a sample of experiments.

VII. INDICATOR SENSITIVITY

Results provided in Section VI validate the performance of the proposed indicator. There are multiple factors that can affect the indicator quality in an industrial environment. Stock and tool mounting conditions, general stiffness of the machine under study, cutting parameters, and tool size can impact the overall machining process. Two major factors are addressed in this section: tool mounting conditions and nonoptimal cutting parameters, i.e., cutting speed, feed rate, RDOC, and ADOC.

A. Tool Holder

There are multiple types of tool holder systems for end mills. An R8 tool holder system was used in the artificial degradation and industrial sample experiment. Cutting operations were repeated using an ER16 tool holder system. The MESbI values for traditional milling and 8-mm end mills are provided in Table V.

Results in Table V validate the performance of the MESbI for an ER16 tool holder system. The proposed indicator performed well with two widely used tool mounting solutions.

B. Nonoptimal Chip Load

Optimal chip load parameters are often tabulated by tool manufacturers. For an RDOC less than the full radius of the tool, the feed rate must be adapted to avoid chip thinning [29]. The adjustment of the feed rate avoids rubbing and maintains the desired material removal rate (MRR) [29]. Although nonoptimal cutting parameters are undesirable, the proposed indicator is verified in such a scenario. Fig. 15 presents the MES for six cutting scenarios of an 8-mm end mill. The first row presents an analysis for cuts with traditional milling parameters. The second row presents data for cuts with HEM milling parameters. The last bar plot in the first row and the middle bar plot in the second row in Fig. 15 correspond to cuts with optimal chip load, Cut 1 and Cut 4 from Table II. The other columns present data for cuts with nonoptimal chip load. Presented results verify that the MES, and consequently the MESbI, perform well for nonoptimal cutting configuration.

The failure to maintain optimal cutting parameters can cause premature tool failure. A cutting scenario with RDOC of 10%,

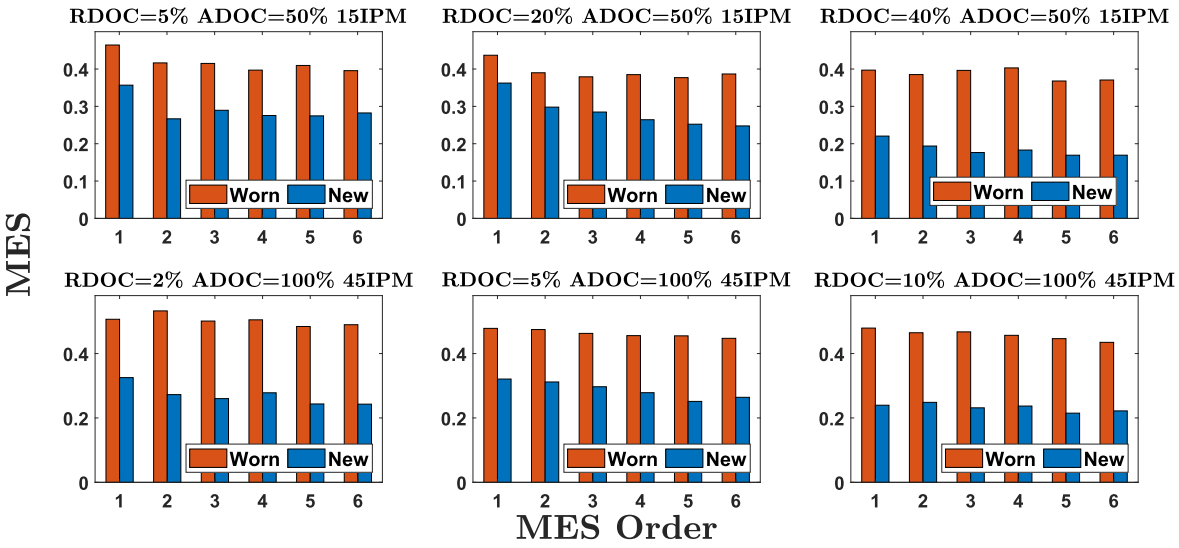

Fig. 15. Nonoptimal cutting configuration.

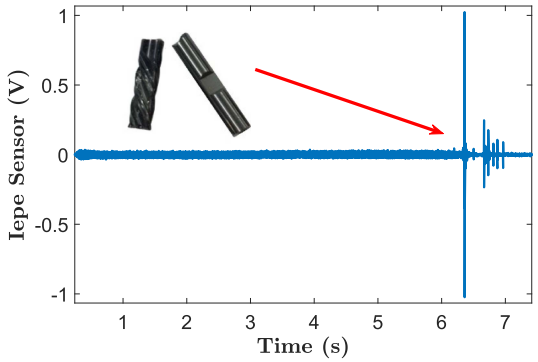

Fig. 16. Tool damage with nonoptimal cutting parameters.

ADOC of 100% and 45 IPM feed rate resulted in the end mill breakage. The instant of tool damage is marked in the vibration data in Fig. 16.

VIII. Conclusion

An instrumentation and measurement solution with custom hardware and tailored signal processing for machine condition monitoring has been developed in this article. The specific application was made to end mill condition monitoring, but many other periodic electromechanical systems could be tracked with the hardware and analytical approach presented here. The methods developed in this article avoid synchronous sampling. The approach presented here is highly sensitive to periodicities and modulation, and can pick up these signatures when sensing is mechanically distanced from the cutting zone.

The state-of-the-art hardware, IoT connectivity, and signal processing algorithm provide actionable information for diagnostic systems. The developed instrumentation system is compact and allows quick and temporary installation as demonstrated in the experimental setup. The signal processing algorithm utilizes cyclostationary analysis to reveal underlying modulation in vibration signals. Practical limitations such as sensor location, tool holder technology, and machining approach were taken into account. The hardware system is characterized by a lack of troublesome equipment, such as quadrature encoders, dynamometers, or optical sensors. The proposed diagnostic indicator MESbI provides a quantity which can be employed to detect tool degradation. A normalized scalar indicator was missing in cyclostationary-based TCM literature. The MESbI was tested on a sample of industrially-worn end mills, a realistic test case often overlooked. The MESbI provided exceptional and repeatable performance as verified by the indicator distribution over multiple tests.

References

[1] D. Kong, Y. Chen, N. Li, C. Duan, L. Lu, and D. Chen, "Tool wear estimation in end milling of titanium alloy using NPE and a novel WOA-SVM model," *IEEE Trans. Instrum. Meas.*, vol. 69, no. 7, pp. 5219–5232, Jul. 2020.

[2] J.-H. Zhou, C. K. Pang, Z.-W. Zhong, and F. L. Lewis, "Tool wear monitoring using acoustic emissions by dominant-feature identification," *IEEE Trans. Instrum. Meas.*, vol. 60, no. 2, pp. 547–559, Feb. 2011.

[3] C. Zhou, Z. Jiang, C. Sun, and Z. Zhu, "The monitoring of milling tool tipping by estimating holder exponents of vibration," *IEEE Access*, vol. 8, pp. 96661–96668, 2020.

[4] L. Zhang, R. X. Gao, and K. B. Lee, "Spindle health diagnosis based on analytic wavelet enveloping," *IEEE Trans. Instrum. Meas.*, vol. 55, no. 5, pp. 1850–1858, Oct. 2006.

[5] S. S. Aralikatti, K. N. Ravikumar, and H. Kumar, "Fault diagnosis of single point cutting tool using spectrum, cepstrum and wavelet analysis," *AIP Conf. Proc.*, vol. 2200, no. 1, 2019, Art. no. 020048.

[6] K. Ait-Sghir, M. E. Badaoui, F. Guillet, D. Aboutajdine, and J.-P. Dron, "Application of the cyclostationairity for the cutting tool diagnosis," *Mech. Ind.*, vol. 15, no. 6, pp. 497–507, 2014.

[7] L. N. L. Lopezdelacalle, A. Lamikiz, J. A. Sanchez, and I. F. FernandezdeBustos, "Simultaneous measurement of forces and machine tool position for diagnostic of machining tests," *IEEE Trans. Instrum. Meas.*, vol. 54, no. 6, pp. 2329–2335, Dec. 2005.

[8] R. G. Lins, B. Guerreiro, P. R. Marques de Araujo, and R. Schmitt, "In-process tool wear measurement system based on image analysis for CNC drilling machines," *IEEE Trans. Instrum. Meas.*, vol. 69, no. 8, pp. 5579–5588, Aug. 2020.

[9] P. S. Pai and P. K. R. Rao, "Acoustic emission analysis for tool wear monitoring in face milling," *Int. J. Prod. Res.*, vol. 40, no. 5, pp. 1081–1093, Jan. 2002.

[10] Y. Zhou and W. Xue, "Review of tool condition monitoring methods in milling processes," *Int. J. Adv. Manuf. Technol.*, vol. 96, nos. 5–8, pp. 2509–2523, May 2018.
[11] C. Zhou *et al.*, "Vibration singularity analysis for milling tool condition monitoring," *Int. J. Mech. Sci.*, vol. 166, Jan. 2020, Art. no. 105254.
[12] D. J. Jin and E. Eisner, "A review of homomorphic deconvolution," *Rev. Geophys.*, vol. 22, no. 3, pp. 255–263, 1984.
[13] A. V. Oppenheim, "Superposition in a class of nonlinear systems," Massachusetts Inst. Technol. Res. Lab. Electron., Cambridge, MA, USA, Tech. Rep. 432, Mar. 1965.
[14] K. Ait sghir, R. Randall, M. El badaoui, and F. Guillet, "Milling cutting tool diagnosis using comparisons of the excitation identified by cepstral techniques," in *Proc. 5th Australas. Congr. Appl. Mech.*, Dec. 2007, pp. 1–5.
[15] J. Antoni, "Cyclostationarity by examples," *Mech. Syst. Signal Process.*, vol. 23, no. 4, pp. 987–1036, May 2009.
[16] M. Lamraoui, M. Thomas, and M. El Badaoui, "Cyclostationarity approach for monitoring chatter and tool wear in high speed milling," *Mech. Syst. Signal Process.*, vol. 44, nos. 1–2, pp. 177–198, Feb. 2014.
[17] Y. Calleecharan, "Spectral analysis and second-order cyclostationary analysis of the non-stationary stochastic motion of a boring bar on a lathe," *Balkan J. Electr. Comput. Eng.*, vol. 3, no. 3, pp. 103–114, Dec. 2015.
[18] S. Guo, T. Yang, W. Gao, and C. Zhang, "A novel fault diagnosis method for rotating machinery based on a convolutional neural network," *Sensors*, vol. 18, no. 5, p. 1429, May 2018.
[19] X. Wu, Y. Liu, X. Zhou, and A. Mou, "Automatic identification of tool wear based on convolutional neural network in face milling process," *Sensors*, vol. 19, no. 18, p. 3817, Sep. 2019.
[20] B. Yang, R. Liu, and E. Zio, "Remaining useful life prediction based on a double-convolutional neural network architecture," *IEEE Trans. Ind. Electron.*, vol. 66, no. 12, pp. 9521–9530, Dec. 2019.
[21] J. Antoni, "Cyclic spectral analysis of rolling-element bearing signals: Facts and fictions," *J. Sound Vib.*, vol. 304, nos. 3–5, pp. 497–529, Jul. 2007.
[22] L. Huchel, J. Helsen, P. A. Lindahl, and S. B. Leeb, "Diagnostics for periodically excited actuators," *IEEE Trans. Instrum. Meas.*, vol. 69, no. 7, pp. 4145–4153, Jul. 2020.
[23] W. Gardner, "Measurement of spectral correlation," *IEEE Trans. Acoust., Speech, Signal Process.*, vol. 34, no. 5, pp. 1111–1123, Oct. 1986.
[24] W. A. Gardner, *Introduction to Random Processes with Applicarion to Signals System*. New York, NY, USA: Macmillan, 1986.
[25] W. A. Gardner, *Statistical Spectral Analysis: A Nonprobabilistic Theory*. Englewood Cliffs, NJ: Prentice-Hall, 1988.
[26] J. Antoni, G. Xin, and N. Hamzaoui, "Fast computation of the spectral correlation," *Mech. Syst. Signal Process.*, vol. 92, pp. 248–277, Aug. 2017.
[27] A. V. Oppenheim and R. W. Schafer, *Discrete Time Signal Processing*. London, U.K.: Pearson, 2013.
[28] *IEPE Vibration Sensor Interface Reference Design for PLC Analog Input*, Texas Instrum., Dallas, TX, USA, 2017.
[29] *HEM Guidebook*. Harvey Performance Company, Rowley, MA, USA, 2017.

Łukasz Huchel received the B.Sc. degree in electrical power engineering from the Silesian University of Technology, Gliwice, Poland, in 2013, and the M.Sc. degree from the Department of Electrical Engineering and Computer Science (EECS), Masdar Institute of Science and Technology, Abu Dhabi, United Arab Emirates, in 2015. He is currently pursuing the Ph.D. degree in EECS with the Massachusetts Institute of Technology, Cambridge, MA, USA.

His current research interests include the development of signal processing algorithms, and hardware and software solutions for condition monitoring and diagnostics.

Thomas C. Krause received the B.S. degree in electrical engineering from Purdue University, West Lafayette, IN, USA, in 2019. He is currently pursuing the Ph.D. degree in electrical engineering and computer science with the Massachusetts Institute of Technology, Cambridge, MA, USA.

His current research interests include the development of signal processing algorithms and sensors for energy and condition monitoring.

Tomasz Ługowski received the B.Sc. degree in automation and robotics from the University of Bielsko-Biała (Akademia Techniczno-Humanistyczna w Bielsku-Białej), Bielsko-Biała, Poland, in 2015.

He is currently managing a company that designs and implements industrial automation systems.

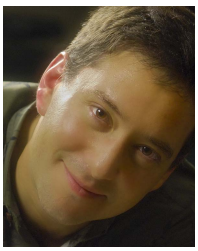

Steven B. Leeb (Fellow, IEEE) received the doctoral degree from the Massachusetts Institute of Technology (MIT), Cambridge, MA, USA, in 1993.

He has served as a Commissioned Officer with the USAF reserves, and he has been a member of the MIT faculty with the Department of Electrical Engineering and Computer Science since 1993. He also holds a joint appointment in MIT's Department of Mechanical Engineering. He is the author or coauthor of over 200 publications and 20 U.S. Patents in the fields of electromechanics and power electronics.

Jan Helsen received the M.Sc. degree in electromechanical engineering and the Ph.D. degree from Katholieke Universiteit Leuven, Leuven, Belgium, in 2007 and 2012, respectively. His Ph.D. thesis was focused on the dynamic simulation of wind turbine gearboxes.

He is currently a Professor with the Acoustics and Vibrations Research Group, Vrije Universiteit Brussel, Brussel, Belgium. His current research interest includes condition monitoring of rotating systems.